The published version of this paper can b found at https://doi.org/10.1007/s11069-021-04977-2

Estimation of maximum seasonal tropical cyclone damage in the Atlantic using climate models.

Sally L. Lavender[1], Kevin J. E. Walsh[2], Steven Utembe[2,3], Louis-Philippe Caron[4], Mark Guishard[5]

[1]Centre for Applied Climate Sciences, University of Southern Queensland, Toowoomba, Queensland, Australia

[2]School of Earth Sciences, University of Melbourne, Parkville, Australia

[3]Environmental Protection Authority Victoria, Melbourne, Australia

[4]Barcelona Supercomputing Centre, Barcelona, Spain

[5]Bermuda Weather Service, Bermuda

Corresponding author: Sally.Lavender@usq.edu.au

Submitted to Natural Hazards

19 Abstract

20 There are several different estimates of the observed cyclone damage potential of tropical
21 cyclones based on observations of size, intensity and track. For the analysis of climate model
22 data, previous work identified an index, the cyclone damage potential climate index
23 ($CDP_{Climate}$), based on relative sea surface temperature (SST) and tropical cyclone steering
24 flow to estimate the damage potential in climate models. Using millennia-long climate
25 models, $CDP_{Climate}$ is estimated for the north Atlantic basin and compared against values from
26 reanalyses and the observed damage potential. The peak in SSTs in the cyclone main
27 development region with respect to the tropical mean SSTs is smaller in these models than
28 reanalyses, resulting in smaller variations in $CDP_{Climate}$.

29 Although the year 1995 had the highest observed cyclone damage potential, the year 2010 is
30 a maximum for $CDP_{Climate}$ in the reanalysis data. The models exceed this 2010 value in less
31 than 1% of model years. Using a model with 100 ensemble members the variability in
32 $CDP_{Climate}$ is examined further. The interannual variability of the ensemble-mean results have
33 a very high correlation (R=0.95) with reanalyses. The high decadal variability is evident and
34 interannual variability is found to have increased during the 30 years after 1981 relative to
35 those prior. The 2010 ensemble-mean value is exceeded in other years by individual
36 ensemble members 1.1% of the time.

37 The results from this study suggest that although it is possible to exceed the observed CDP,
38 this is rare in the current climate. However, this study doesn't consider changes as we move
39 to future climates.

40

41

42 Keywords: tropical cyclones, north Atlantic, damage potential, climate models

1. Introduction

Natural hazard managers and policymakers need the best possible information regarding the recurrence intervals of hazards such as tropical cyclones (TCs). Lavender et al. (2018) examined the question of whether the large number of TCs that occurred in the Atlantic basin in 2005 could serve as an approximate upper limit for TC incidence in this basin. However, this previous study did not examine the total destructive potential of TCs through seasonal measures of TC intensity. TC damage scales non-linearly with intensity and, while there is some correlation between the number of storms and measures of intensity, this correlation is not perfect (e.g. Misra et al. 2013). For instance, when the TC risk is measured by Accumulated Cyclone Energy (ACE; Bell et al. 2000; see the Appendix), the year 1995 (with 19 TCs) approaches the values in the year 2005 (with 28 TCs). The year 2020 had an extraordinarily high number of TCs (30) but ACE was lower than in 1995.

There are various integrated measures that have been developed as a way of categorizing the cumulative activity of TCs over a season (see the Appendix for definitions of these indices). These include ACE, Total Integrated Kinetic Energy (TIKE; Powell and Reinhold 2007; Misra et al. 2013), the Power Dissipation Index (PDI; Emanuel 2005), and the Cyclone Damage Potential (CDP; Holland et al. 2019). In particular, the work of Villarini and Vecchi (2012), Misra et al. (2013) and Done et al. (2018) has shown that it is possible to establish relationships between seasonal average climate conditions and indices related to damage potential. Thus the total damage potential for a season may be calculated from long climate model simulations as a way of estimating long-term variations in damage-related TC intensity indices.

Following on from Lavender et al. (2018), the present study analyses long climate model simulations of the current climate (Hunt and Watterson 2010; Hazeleger et al. 2012) and

67 determines the year-to-year variations in climate conditions that are associated with changes
68 in TC intensity indices. The models to be examined are coupled ocean-atmosphere models
69 which generate their own climate variability. Lavender et al. (2018) showed that these models
70 provide a good representation of the typical observed variation of climate parameters
71 previously associated with TC formation. This suggests they are suitable to analyse climate
72 parameters associated with TC intensity indices, such as those parameters employed in Done
73 et al. (2018).

74 Even with the same forcing sea surface temperatures, the randomness inherent in the climate
75 system may result in different atmospheric climate states. This would then affect the possible
76 values of the TC intensity indices generated even with the same climate conditions.
77 Accordingly, simulations using a higher-resolution model, the Japanese MRI-AGCM (Mizuta
78 et al. 2012), will be used for this purpose, as in Lavender et al. (2018). This model has
79 simulated 100 different "realizations" or possible atmospheric states for the period 1951-
80 2011, forced by the observed sea surface temperature conditions over that time period. The
81 variations in TC intensity indices between ensemble members will be examined as a way of
82 quantifying the spread in atmospheric states related to TC intensity that could occur given a
83 possible set of climate conditions. In addition, these more modern climate simulations are of
84 finer resolution than the millennial simulations and thus provide an additional source of long
85 climate model output (100 realizations of 61 years each, giving 6,100 years of model output)
86 that can be compared with the other models.

87 The assessment of risk is crucial to the insurance and reinsurance industries (e.g., Collins and
88 Walsh 2019). In particular, an assessment of the maximum possible risk for a particular
89 hazard in a particular region with high vulnerability would be of considerable utility. An
90 estimate of the maximum TC incidence in the Atlantic basin has already been reported
91 (Lavender et al. 2018). Building on this work, we aim to analyze millennial climate model

simulations to determine the variations in Atlantic intensity indices and damage potential. These will be compared with the seasonal integrated TC intensity for 2005 and other years of high integrated intensity in the observed record, to determine whether a risk assessment benchmark for damage potential could be established.

2. Data and Method

2.1. Observational data

Observed TC data for the North Atlantic region come from the Extended Best Track dataset (EBTrACS; Demuth et al. 2006) for the period 1988-2019. This extended best track dataset supplements the Atlantic hurricane database (HURDAT2; Landsea and Franklin 2013) by including radial extent of 64 kt winds for the years 1988—2003 prior to this being included in HURDAT2. Additionally, it includes the radius of maximum wind speed (Rmax). Due to the extremely active 2020 season, the analysis was extended to include the year 2020, however these tracks were obtained directly from HURDAT2 so do not include Rmax.

Sea surface temperature data are taken from the Hadley Centre Sea Ice and Sea Surface Temperature data set (HadISST; Rayner et al. 2003) at one-degree resolution over the 1988-2020 period. *Relative SST* ($SST_{relative}$) is calculated using the definition of Done et al. (2018) as the difference between the SST averaged over the region 5-20N and 60-15W and the SST over the global tropics within 15S and 15N. *Observed atmospheric data* are taken from two different "reanalysis" data sets, a blended product of both observations and weather forecast model output: ERA5 (Hersbach et al. 2020) for the period 1979—2020 and Modern-Era Retrospective analysis for Research and Applications, Version 2 (MERRA2; Gelaro et al. 2017) for the period 1980—2020. *Steering flow* (STR), the wind speed and direction that is

most influential for TC movement, is defined here as the pressure-weighted integral of the zonal and meridional winds at 850, 700, 500 and 300 hPa (e.g., Galarneau and Davis 2013).

2.2. Observed storm metrics

The damage potential of TCs can be estimated using a number of different metrics, as documented in the equations in the Appendix. Timeseries of annual accumulated values of these metrics are shown in Fig. 1 for the period 1988—2020, as a way of putting the subsequent analysis in this paper into the context of previous work on damage indices. ACE and PDI (eqns. 2 and 3 in the Appendix) are both highly correlated with the number of TCs (R=0.7 and R=0.62 respectively) with year 2005 a maxima in both metrics. However, these metrics only depend on the intensity of the storm and duration and do not take account of the size of the storm or how long it is impacting a region. Prior to wind radii data becoming available, these indices provided our best estimate of the potential damage of a TC. However, since the advent of the recording of wind radii data, other metrics have been developed to better represent total energy e.g. TIKE (equation 4) and CDP (equation 5). These both include a measurement of size, with CDP also including translational speed. Since TIKE is dependent on Rmax, here this is only calculated up to the 2019 season. The year 1995 had the largest CDP and TIKE values but only 19 named storms compared with 28 in the extremely active year 2005. The lower values of CDP and TIKE for 2005 suggest more smaller and less intense TCs during that year. The year 2020 was extraordinary with 30 TCs but the values of CDP remain much lower than some years that had almost half the number of storms. For the present study, we use 1995 as the maximum observed TC damage over this relatively short period of observations, due to our use of an index based on CDP to be applied to our climate model results.

2.3. Calculation of $CDP_{Climate}$

Done et al. (2018) developed an index for North Atlantic TC damage potential, $CDP_{Climate}$ (their equation 2) from large-scale climate variables. This index is an approximation to the CDP index derived from TC observations using climate variables. The advantage of such an index is that it can easily provide a first guess estimate of cyclone-related damages based on reanalysis and the most commonly available climate model output. This is different to the genesis indices used in Lavender et al. (2018) which are an estimation of the number of TCs per year rather than the associated damage. However, there will be similarities between $CDP_{Climate}$ and the genesis indices since both are dependent on favourable environmental conditions. Based on the observational CDP, the maximum wind speed and radius of hurricane force wind were both found to correlate well with relative SST and the translational speed was found to correlate with the weighted steering flow (whereby weighting is by the TC track density). The index was calculated over an extended main development region (EMDR; 5-20N, 60-15W) during the months of August, September, October (ASO). Done et al (2018) used seeding of passive tracers in the 6 hourly large-scale flow to estimate the track density in order to weight the steering flow. The use of millennia-long climate models in the current study means we do not have the 6-hourly data required for the seeding. Instead it was decided (James Done, private communication, 2018) to use the climatological track density from observations to weight the steering flow. This will mean the weighting is the same across all data but is preferred to the use of genesis indices which can give a poor spatial distribution of genesis (e.g. Emanuel and Nolan 2004; Bruyère et al. 2012).

Although the functional relationships in the $CDP_{Climate}$ index as defined by Done et al. (2018) are found to hold true, the coefficients in the equation are adjusted to give a better fit between

the observed CDP and $CDP_{Climate}$, such that a modified equation (Eqn. 1) is used in the present study:

$$CDP_{Climate} = 20\frac{SST_{relative}}{STR_w} \quad (1)$$

Here the value of the coefficient is determined by minimising root mean square error (RMSE) values between $CDP_{Climate}$ calculated in both ERA5 and MERRA2 and observed CDP. In testing this index different regions and seasons were examined. For the remainder of this paper the EMDR (5-20N, 60-15W) and ASO were used, consistent with Done et al. (2018).

2.4. Climate model data

Three climate models are analysed in this study. The first two are millenia-long climate model simulations produced by the CSIRO Mk2 coupled ocean-atmosphere climate model (Gordon and O'Farrell, 1997) analyzed for 5000 years and the EC-Earth coupled model (Hazeleger et al., 2012) analyzed for 1000 years. The CSIRO model is run with a fixed CO_2 concentration of 330 ppm while the EC-Earth model is a "last millenium" simulation that uses assumptions about varying solar and greenhouse forcing during the period from 850 to 1850 CE (Zhang et al. 2021) . The final model is the Meteorological Research Institute AGCM, version 3.2 (MRI-AGCM3.2; Mizuta et al. 2012, Mizuta et al. 2017). An important difference in the model setup for this model compared with that for the CSIRO and EC-Earth models is that the MRI model is forced with observed SSTs. Observed interannually-varying greenhouse gas concentrations are used in this set of simulations. For the different ensemble members, different initial conditions for the atmosphere and small SST perturbations were used. Random SST perturbations of up to 30% of the observed interannual variability are added to the observational data to account for observational uncertainties, as described in detail in Mizuta et al. (2017). The resulting variability across all the ensemble members

187 gives a good indication of the internal variability of the model. All 100 ensembles for the 61
188 year (1951—2011) period are analyzed to determine whether, given exactly the same climate
189 forcing, random variation in formation rates could cause years of high $CDP_{Climate}$.
190

191 2.5. Variance scaling

192 The values of $CDP_{climate}$ from the millennial climate models were found to show much less
193 variability than observed, consistent with the findings using the same models for TC genesis
194 indices (statistical relationships between climate variables and TC formation; Lavender et al.,
195 2018). To address this issue, we rescaled the variance of $CDP_{climate}$ to match the variance of
196 $CDP_{climate}$ when it is applied to ERA5 reanalyses. The timeseries of $CDP_{climate}$ derived from a
197 climate model was divided by its standard deviation and this standardised time series was
198 multiplied by the standard deviation of the $CDP_{climate}$ ERA5 timeseries. The mean is then also
199 adjusted again to match the observed timeseries. The adjusted $CDP_{climate}$ will have the same
200 mean and magnitude of variance, but how the timeseries varies year-to-year will be
201 dependent on the individual data set to which the $CPD_{climate}$ metric is applied. Thus we make
202 no *a priori* assumption about the statistical distribution of the resulting data; the distribution
203 is whatever is simulated by the model. Adjusting the variance of the simulated $CDP_{climate}$ time
204 series should provide a more adequate comparison to observations of the distribution
205 obtained from the different climate models. We note that one of the limitations of this method
206 is that we get some years with negative values, which is unphysical. Nevertheless, the
207 number of years with negative values is considerably less than 1%.

208 An alternative method would be to match the variance of the $CDP_{climate}$ values from the
209 climate models to observed CDP and then compare the $CDP_{climate}$ values from the climate
210 models to observed CDP. The main drawback of this method is that it might be affected more

strongly by stochastic variability of TC formation than comparing $CDP_{climate}$ model output to $CDP_{climate}$ from ERA5, given the relatively short period of the training data set (a couple of decades). Such a comparison might give an inflated estimate of the actual observed variance. Along these lines, test results with this method showed a large number of negative $CDP_{climate}$ values from the climate models in the resulting histograms (not shown). It was therefore decided to use the more conservative scaling whereby the climate model variances were scaled to the variance of the $CDP_{climate}$ from ERA5.

Note that because of this scaling method, the climate models are therefore not used directly to obtain an improved estimate of the mean and variance of TC damage. In our study, the advantage of the climate model simulations is their extreme length (thousands of years) and the fact that we make no assumption about the distribution or return period of extremes of the model output. This enables them to generate extremes of the distribution in a physically consistent fashion, due to their internally consistent representation of the climate conditions associated with TCs.

3. Comparison of $CDP_{Climate}$ with observed CDP

Timeseries of observed CDP, accumulated over the North Atlantic basin during ASO and $CDP_{Climate}$ calculated from ERA5 and MERRA2 over the EMDR during ASO for the period 1988-2020 are presented in Fig. 2. For reference, ASO averaged relative SST from HadISST is also shown. For the 1988—2009 period analysed by Done et al. (2018) we find a similar correlation as their study with $CDP_{Climate}$ calculated in ERA5 (MERRA2) explaining 49% (52%) of the variability of observed CDP. There are differences between the observed CDP in the two studies, likely due to updates to the TC database since the earlier analysis was done. Over the full period used in the current study the correlation drops so that only 26%

(28%) of the variability of observed CDP can be explained (R=0.51 (0.53)). This is statistically significant at the 99% confidence level (p-value=0.002). Using Spearman rank correlations, the variance explained is increased by 2—3%. $CDP_{Climate}$ (equation 2) is highly dependent on the relative SST so during periods of time where the relationship between observed CDP and relative SST breaks down we get a lower correlation. For example, the year 2010 had a high relative SST leading to a maxima in $CDP_{Climate}$ but the observed CDP was low, whereas 2017 had low relative SST and had a high CDP in the observed record. Although the relationship is not as strong in recent years, this metric is the best estimate we currently have for analysing the potential cyclone damage from the model data over the North Atlantic. The next section analyses the values of $CDP_{Climate}$ calculated from model data.

4. Modelled results

Without any scaling applied, the CSIRO model had a mean $CDP_{Climate}$ of 3.9 and EC-Earth had a much lower value of 0.5. The differences between the two models can be attributed to higher values of SST, and hence relative SST, in the EMDR region in the CSIRO model compared with the EC-Earth model (Figure 3). The relative SST averaged over the EMDR has a mean of just 0.06 K in EC-Earth, an order of magnitude smaller than that from CSIRO (0.69 K) which is very close to the observed value of 0.70. Based on equation 1 we would expect this to result in much smaller values of $CDP_{Climate}$ in EC-Earth. The mean of $CDP_{Climate}$ from the MRI model over all 100 ensembles and 61 years is 3.7, which is the closest model to both the observed mean CDP (3.6) and $CDP_{Climate}$ calculated in ERA5 (3.2) and MERRA2 (3.1). Figure 4 shows the interannual variability in $CDP_{Climate}$ calculated in these models. The EC-Earth and CSIRO models have standard deviations in the range 0.8—0.9, compared to 1.4 for $CDP_{Climate}$ in both ERA5 and MERRA2, and 2.5 in observed CDP. This limited

interannual variability is due to a lower variability in relative SST over the EMDR in the models relative to both reanalyses and observations and was also found when calculating the modelled genesis indices (Lavender et al., 2018). In the Lavender et al. (2018) study, the ERA and modelled results were variance-scaled to observed values. However, in the present study, to remain comparable with Done et al. (2018) the ERA5 data are not scaled and the values of $CDP_{Climate}$ from the models are instead variance scaled to ERA5. We are then able to compare the maxima in the climate models with those in ERA5. The MRI model has a smaller standard deviation than ERA5 with the ensemble mean having a standard deviation of 1.1. When all individual ensemble members are considered, there is an average (taken over all 100 ensembles) over the 61 year period of 1.2, varying between 1.0 and 1.5. The values of $CDP_{Climate}$ are shown in the histogram in Fig. 5 for ERA5, MERRA2 and the variance-scaled climate model data. For direct comparison in this figure the individual MRI ensembles have been variance-scaled to ERA5 as with the other models. The maximum ERA5 value (7.1) is exceeded by all models but only rarely. The variance scaled $CDP_{Climate}$ values from CSIRO and EC-Earth exceed the 2010 ERA5 maxima only 0.2 % (11) and 0.6% (6) of the time, with percentage exceedance of 12% (8.0) and 24% (8.8) respectively. The variance scaled $CDP_{Climate}$ values from all MRI ensembles exceed this value in 1.0% (59) of years with a maximum percentage exceedance of 28% (9.1). When we consider the year 1995 which has the second highest $CDP_{Climate}$ in ERA5 and the highest observational CDP, the ERA5 value of $CDP_{Climate}$ (5.2) is exceeded in 7—8% of model years (406, 74 and 493 times by the CSIRO, EC-Earth and MRI models respectively).

One caveat here is that the $CDP_{Climate}$ values as diagnosed from ERA5 or MERRA2 can underestimate the actual observed CDP values for individual years. For instance, in 1995, the observed CDP value was 10, whereas this extreme value is not seen in Fig. 2. A fundamental issue here is one that was previously identified in Lavender et al. (2018): due to stochastic

284 factors associated with the development of individual TCs, even given the same atmospheric
285 climate, two different years can have two different observed CDP values. This stochastic
286 interannual variability has been estimated to be as much as 40% of the variance (Done et al.
287 2014; Lavender et al. 2018). This issue is addressed using the MRI model: 100 ensemble
288 members each using the observed SSTs but with different perturbations of initial atmospheric
289 conditions and SSTs. This allows us to examine the breadth of possible $CDP_{Climate}$ values due
290 to this stochastic behaviour. Since the mean variance of interannual variability in the MRI
291 model is comparable to ERA5 it is not necessary to variance-scale this data and thus we
292 retain the different variances in the different ensembles. Instead we simply adjust the mean
293 of each ensemble member over the 61-year period to be equal to that from ERA5 (3.2). A
294 timeseries of the ERA5 and MRI ensemble mean $CDP_{Climate}$ is shown in Fig. 6 along with all
295 the individual ensemble members. The standard deviation for each year is shown by the
296 dotted line in Fig 6. This has a mean value of 0.48, varying between 0.31 (in 1972) and 0.75
297 (in 2010) suggesting stochastic variability in the range of 26% to 63%, where stochastic
298 variability is calculated as the standard deviation in a particular year divided by standard
299 deviation over all years (1.2). This is consistent with previous studies (Lavender et al. 2018;
300 Done et al. 2014). Although the mean MRI $CDP_{Climate}$ is highly correlated (R=0.95) with
301 ERA5, all years have ensemble members that exceed the ERA5 value, showing that
302 stochastic variability is important and small changes to the atmosphere and SST can result in
303 higher TC damage under current climate conditions. Ideally, an estimate of the stochastic
304 atmospheric variability in the CSIRO and EC-Earth models could be obtained by using the
305 same experimental design as used for the MRI model, but such simulations were not
306 available.

307 There are several other points to note about this result. It has been previously established that
308 there is substantial decadal variability of TC incidence in this basin (Landsea et al. 1999;

Goldenberg et al. 2001; Patricola et al. 2014) and this is also indicated in Fig. 6. After a relatively quiescent period in in 1970s and 1980s, after the mid 1990s, $CDP_{Climate}$ returns to the higher values more typical of the 1950s. For instance, while highest ensemble mean $CDP_{Climate}$ values occur in 2010 (6.3), values in 1955 (5.4) were the second highest. The interannual variability has increased during the more recent period with the ensemble mean having a standard deviation of 1.3 when calculated over the years after 1981 compared to 0.9 over the years prior.

The year 2010 is maximum in ERA5, MERRA2 and the MRI model due to the high relative SSTs in the MDR during that year. This peak in the mean-adjusted ensemble mean MRI $CDP_{Climate}$ (6.3) is exceeded by a number of ensemble members in years 2005, 1995 and 1955 with an exceedance rate of just 1.1%.

5. Discussion and Conclusion

This analysis suggests that it is possible, although rare, to have years with greater TC damage than has occurred in the observed record between 1988 and 2020. The millennial models (CSIRO and EC-Earth) suggest an exceedance of the ERA5 maxima in less than 0.6% of model years. Using the 100 ensemble members of the MRI model over the 61 years gives us 6100 years of simulation with exceedance of the ERA5 maxima in $CDP_{Climate}$ only in 1.0% of model years. Thus in any given upcoming year, assuming SSTs remain in the historical range, there is rather less than a 1% chance that the TC damage for that year would exceed the maximum TC damage per year that occurred during the period 1988-2020.

There are important uncertainties in this analysis that need to be emphasized. $CDP_{Climate}$ has been formulated from a limited number of years of observations and therefore inevitably has statistical sampling errors associated with the values chosen. Even if a longer observational data set were used, the actual variables incorporated in $CDP_{Climate}$ would likely not be a

complete representation of the relationship between TC damage and atmospheric conditions due to the internal variability of TCs as discussed in the previous section. However, as pointed out by Done et al. (2018), the significant relationship between $CDP_{Climate}$ and observed CDP is encouraging. Additionally, the climate models are not a perfect representation of the real atmosphere, and so their lengthy simulations provide only an approximation of the behaviour of the atmosphere over thousands of years. The comparison in Fig. 4 shows that when applied to reanalyses, the $CDP_{Climate}$ index underestimates the variance of the actual observed CDP. The most likely explanation for this is that the $CDP_{Climate}$ index cannot fully account for the stochastic variability of TC formation and intensity. We also note that there are limitations in the methodology used which are particularly evident in the years post-2009 when the relationship between observed CDP and $CDP_{Climate}$ becomes weaker. This suggests there is something missing from this index and relative SST has recently become less important, for reasons unknown at this stage. Ultimately, the most effective way to account for this apparent shortfall in the stochastic variability of this estimate of TC damage would be to use a fine-resolution coupled ocean-atmosphere climate model that has a good simulation both of observed TC formation rates and intensities, along with a good simulation of the TC-related climate variables discussed above. Such a model could then be run for periods of hundreds or thousands of years, to provide a direct estimate of the possible interannual variation of TC damage. It would also be instructive to compare the results shown here to those that might be obtained from an ensemble of recent CMIP6 models (Eyring et al. 2016), particularly through a comparison of runs with and without historical enhanced greenhouse forcing, to determine the possible impact of the enhanced greenhouse effect to date on any changes in extremes.

A related issue is whether the upward trend in Fig. 6 is due to external forcing or could be generated by internal climate variability alone. Previous analysis of the CSIRO millenial

358 climate simulations has suggested that internal variability alone is capable of producing
359 substantial decadal fluctuations in the climate system (e.g. Hunt 2011, 2012, 2014). A
360 thorough examination of the relative contribution of internal and external forcing to this trend
361 has not been performed at this time, since this study is only concerned with the current
362 climate and not with changes under future climate. Since the index used is highly dependent
363 on relative SST, future changes in this will result in a shift in the relationship between CDP
364 and $CDP_{Climate,}$ and the extent of this shift has not yet been evaluated.

365

366 **APPENDIX**

367 **Accumulated cyclone energy, ACE** (Bell et al. 2000)

368 $$\text{ACE} = \sum v_{\max}^2 \quad (2)$$

369 where v_{max} is the maximum wind speed.

370

371 **Power dissipation index, PDI** (Emanuel 2005)

372 $$\text{PDI} = \int_0^\tau v_{\max}^3 dt \quad (3)$$

373

374

375 **Total integrated kinetic energy, TIKE** (Powell and Reinhold 2007; Misra et al. 2013)

376 The integrated kinetic energy (IKE) integrated over all tropical cyclones in the basin in a
377 season:

378 $$\text{IKE} = \int_v 1/2 \rho A V^2 \quad (4)$$

379 where, ρ is air density (1.15 kg m^{-3}), and A and V are, respectively, the area and mean 10-m
380 wind speed of the contributing portion of the quadrant using equations in Misra et al.'s (2013)
381 Table A1 utilising the radii of 18 m s^{-1}, 26 m s^{-1}, 33 m s^{-1}, and maximum winds (Rmax).

382

383

Cyclone damage potential, CDP (Done et al. 2018)

$$\text{CDP} = 4\frac{\left[\left(\frac{v_m}{65}\right)^3 + 5\left(\frac{R_h}{50}\right)\right]}{v_t} \quad (5)$$

where v_m is the maximum windspeed, R_h is the radius of hurricane winds and v_t is the forward translation speed. This is normalized between 0 and 10 by dividing by the maximum accumulated CDP and multiplying by 10.

Declarations

Funding: This study was funded by Bermuda Institute of Ocean Sciences' Risk Prediction Initiative (RPI). Calculations were performed on the National Computational Infrastructure supercomputer, funded by the Australian Government. SLL is currently funded by Meat and Livestock Australia (MLA), the Queensland Government, and University of Southern Queensland through the Northern Australian Climate Program (NACP). **Conflicts of interest/Competing interests:** None. **Availability of data and material (data transparency):** Data is available upon request from the first three authors. **Code availability (software application or custom code):** Code used in this research can be made available upon request. **Authors' contributions**: KJEW, SLL and L-PC designed the research, SLL and SU performed the analysis with input from KJEW, L-PC and MG. SLL and KJEW wrote the article with input from all other authors.

403 **References**

404 Bell GD, Halpert MS, Schnell RC et al (2000) Climate assessment for 1999. Bull. Amer. Meteorol.
405 Soc., **81**:S1–S50.

406 Bruyère CL, Holland GJ, Towler E (2012) Investigating the use of a genesis potential index for
407 tropical cyclones in the North Atlantic Basin. J. Climate, 25:8611–8626.

408 Collins J, Walsh K (2019) Hurricane Risk. Springer, Cham

409 Demuth J, DeMaria M, Knaff JA (2006) Improvement of advanced microwave sounder unit tropical
410 cyclone intensity and size estimation algorithms. J. Appl. Meteor., 45:1573-1581.

411 Done JM, Bruyère CL, Ge M, Jaye A (2014) Internal variability of North Atlantic tropical cyclones. J.
412 Geophys. Res. Atmos., 119:6506-6519.

413 Done JM, PaiMazumder D, Towler E, Kishtawal CM (2018) Estimating impacts of North Atlantic
414 tropical cyclones using an index of damage potential. Clim. Change, 146:561—573.

415 Emanuel K (2005) Increasing destructiveness of tropical cyclones over the past 30 years, Nature,
416 436:686—688. doi:10.1038/nature03906.

417 Emanuel KA, Nolan DS (2004) Tropical cyclone activity and global climate. In: Proceedings of the
418 26th Conference on Hurricanes and Tropical Meteorology, American Meteorological Society, Miami,
419 FL, 2004, 240–241. Available at:
420 ftp://texmex.mit.edu/pub/emanuel/PAPERS/em_nolan_extended_2004.pdf.

421 Eyring V, Bony S, Meehl GA, Senior CA, Stevens B, Stouffer RJ, Taylor KE (2016) Overview of the
422 Coupled Model Intercomparison Project Phase 6 (CMIP6) experimental design and organization.
423 Geosci. Model Dev., 9:1937-1958. doi:10.5194/gmd-9-1937-2016.

424 Galarneau TJ Jr, Davis CA (2013) Diagnosing forecast errors in tropical cyclone motion. Monthly
425 weather review, 141(2):405-430.

Gelaro R, McCarty W, Suárez MJ et al (2017) The Modern-Era Retrospective Analysis for Research and Applications, Version 2 (MERRA-2). J. Clim. 30:5419—5454. doi: 10.1175/JCLI-D-16-0758.1.

Goldenberg SB, Landsea CW, Mestas-Nuñez AM, Gray WM (2001) The recent increase in Atlantic hurricane activity: Causes and implications. Science, 293(5529):474—479.

Gordon HB, O'Farrell SP (1997) Transient climate change in the CSIRO coupled model with dynamic sea ice. Mon Weather Rev, 125:875–907.

Hazeleger W, Wang X, Severijns C et al (2012) EC-Earth V2. 2: description and validation of a new seamless earth system prediction model. Clim Dyn, 39, 2611-2629.

Hersbach H, Bell B, Berrisford P et al (2020) The ERA5 global reanalysis. Q J R Meteorol Soc, 146:1999–2049. doi:10.1002/qj.3803.

Holland GJ, Done JM, Douglas R, Saville GR, Ge M (2019). Global tropical cyclone damage potential. In J. Collins & K. Walsh (Eds.), Hurricane risk (pp. 23–42). Springer, Cham.

Hunt BG, Watterson IG (2010) The temporal and spatial characteristics of surrogate tropical cyclones from a multimillenial simulation. Clim. Dyn., 34:699-718.

Hunt BG (2011) Global characteristics of pluvial and dry multi- year episodes, with emphasis on megadroughts. Int. J. Climatol., 31:1425-1439.

Hunt BG (2012) Stochastic control of Indian megadroughts and megafloods. Clim. Dyn., 39:1801–1821.

Hunt BG (2014) The influence of stochasticism on Indian summer monsoon rainfall and its impact on prediction. Clim. Dyn., 42(9-10):2271-2285.

Landsea CW, Franklin JL (2013) Atlantic Hurricane Database Uncertainty and Presentation of a New Database Format. Mon. Wea. Rev., 141:3576-3592.

448 Landsea CW, Pielke RA, Mestas-Nunez AM, Knaff JA (1999) Atlantic basin hurricanes: Indices of
449 climatic changes. Climatic change, 42(1):89-129.

450 Lavender SL, Walsh KJE, Caron L-P, King M, Monkiewicz S, Guishard M, Zhang Q, Hunt B (2018)
451 Estimation of the maximum annual number of North Atlantic tropical cyclones using climate models.
452 Sci. Adv., 4(8): eaat6509. doi: 10.1126/sciadv.aat6509.

453 Mizuta R, Yoshimura H, Murakami H et al (2012) Climate simulations using MRI-AGCM3. 2 with
454 20-km grid. J Meteorol Soc Japan. Ser. II, 90:233-258.

455 Mizuta R, Murata A, Ishii M et al (2017) Over 5,000 Years of Ensemble Future Climate Simulations
456 by 60-km Global and 20-km Regional Atmospheric Models. Bull. Amer. Meteor. Soc., 98:1383–
457 1398. https://doi.org/10.1175/BAMS-D-16-0099.1.

458 Misra V, DiNapoli S, Powell M (2013) The track integrated kinetic energy of Atlantic tropical
459 cyclones. Mon Wea Rev, 141:2383-2389.

460 Patricola CM, Saravanan R, Chang P (2014) The impact of the El Niño–Southern Oscillation and
461 Atlantic meridional mode on seasonal Atlantic tropical cyclone activity. Journal of Climate,
462 27(14):5311-5328.

463 Powell MD, Reinhold TA (2007) Tropical cyclone destructive potential by integrated kinetic energy.
464 Bull. Amer. Meteorol. Soc., 88, 513–526.

465 Rayner NA, Parker DE, Horton EB et al (2003) Global analyses of sea surface temperature, sea ice,
466 and night marine air temperature since the late nineteenth century, J. Geophys. Res., 108, 4407.
467 doi:10.1029/2002JD002670.

468 Villarini G, Vecchi GA (2012) North Atlantic power dissipation index (PDI) and accumulated
469 cyclone energy (ACE): Statistical modelling and sensitivity to sea surface temperature changes, J.
470 Climate, 25:625—637.

Zhang Q, Berntell E, Li Q, Ljungqvist FC (2021) Understanding the variability of the rainfall dipole in West Africa using the EC-Earth last millennium simulation. Clim. Dyn., 57:93—107. https://doi.org/10.1007/s00382-021-05696-x

Figures

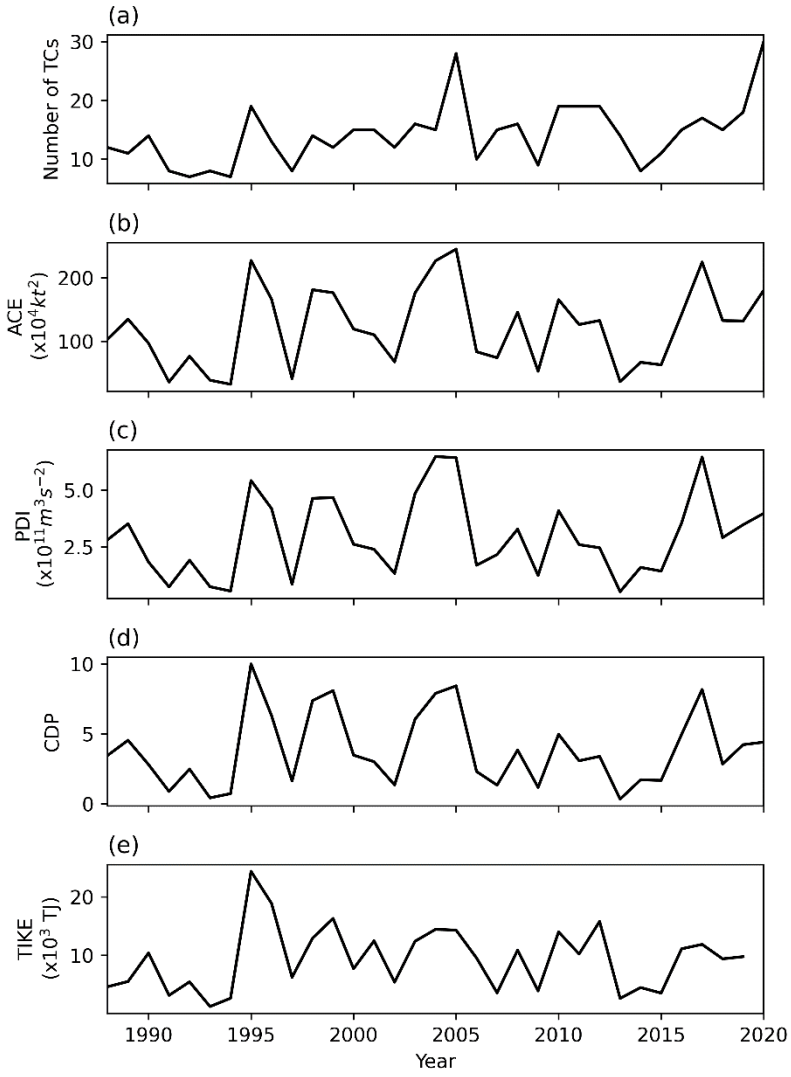

Fig 1 Timeseries for the period 1988—2020 of annually accumulated values over the North Atlantic basin of (a) number of TCs, (b) ACE, (c) PDI, (d) CDP and (e) TIKE. TIKE is only available 1988-2019 due to EBTrACS not yet including values for 2020.

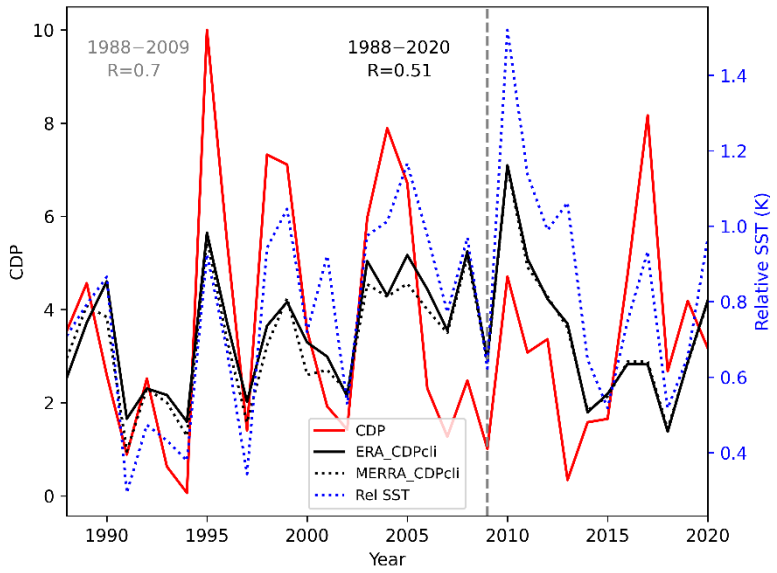

Fig 2 Timeseries of ASO, North Atlantic basin accumulated observed CDP (red line), $CDP_{Climate}$ calculated over the EMDR region during ASO in ERA5 (black line) and MERRA2 (black, dotted line) and average ASO HadISST relative SST (EMDR minus global tropics; blue, dotted line). Correlation coefficients between CDP and ERA5 $CDP_{Climate}$ for the 1988—2009 (grey) and 1988—2020 (black) periods are shown. The vertical dashed line indicates the year 2009.

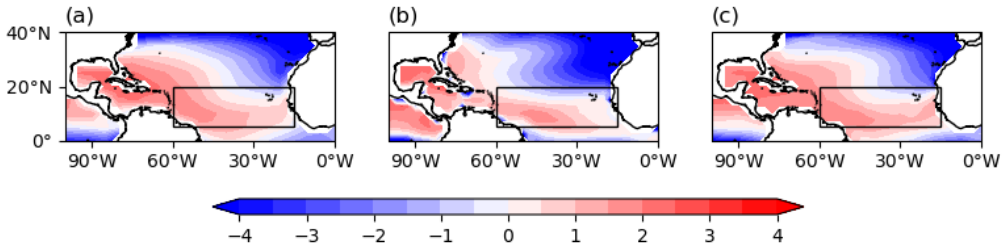

Fig 3 Relative SST averaged over all ASO seasons from (a) CSIRO, (b) EC-Earth and (c) HadISST (1979-2020). The box shows the EMDR region.

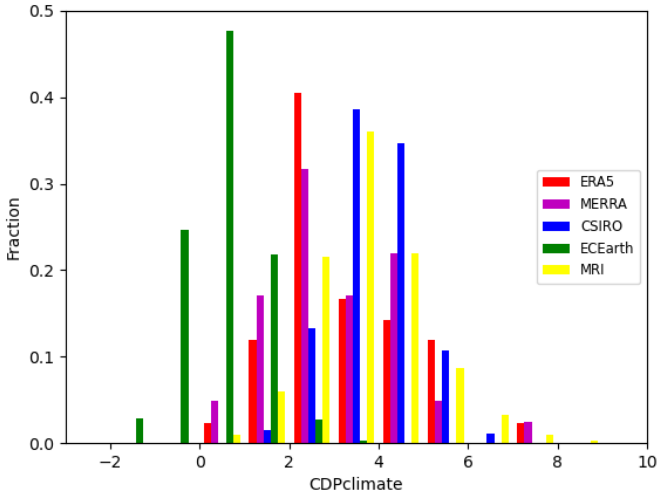

492

493 **Fig 4** Histogram of raw (unscaled) $CDP_{Climate}$ from ERA5 reanalysis (42 years), MERRA2

494 reanalysis (41 years) and CSIRO (5000 years), EC-Earth (1000 years) and MRI (100

495 ensembles; 61 years) models. All calculated over the EMDR region during ASO.

496

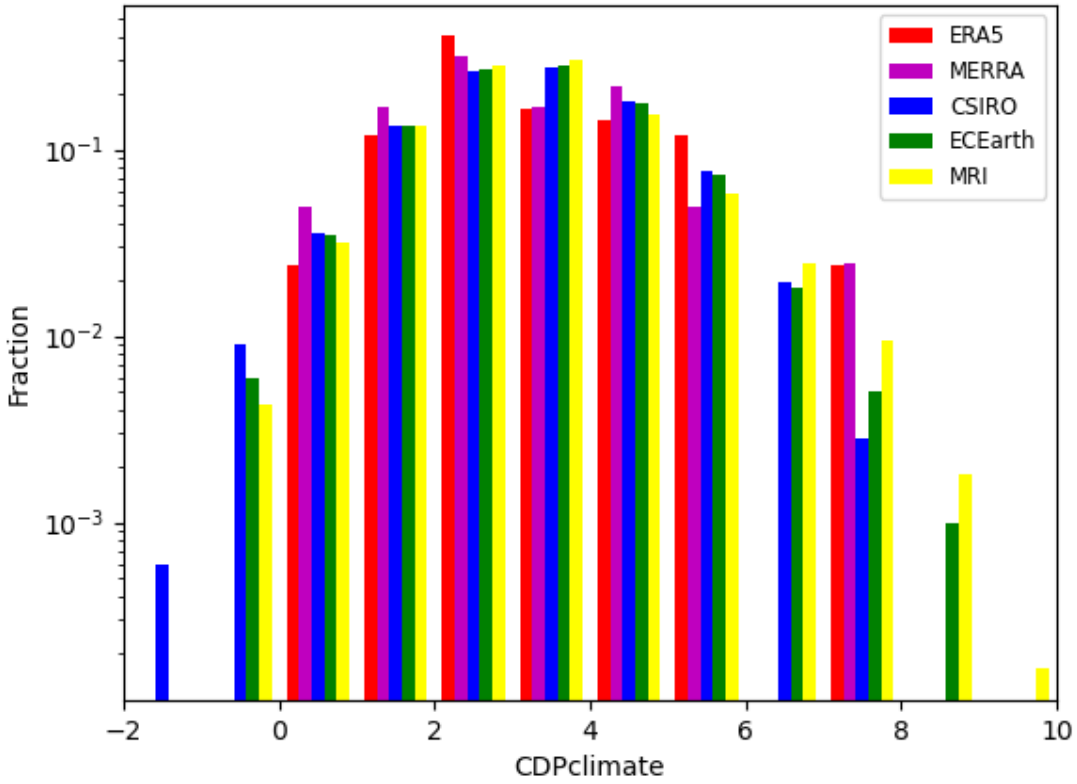

Fig. 5 Histogram of normalised $CDP_{Climate}$ calculated over the EMDR region during ASO. Note the log-scale on the y-axis. The CSIRO, EC-Earth and MRI data have been variance-scaled to the ERA5 data.

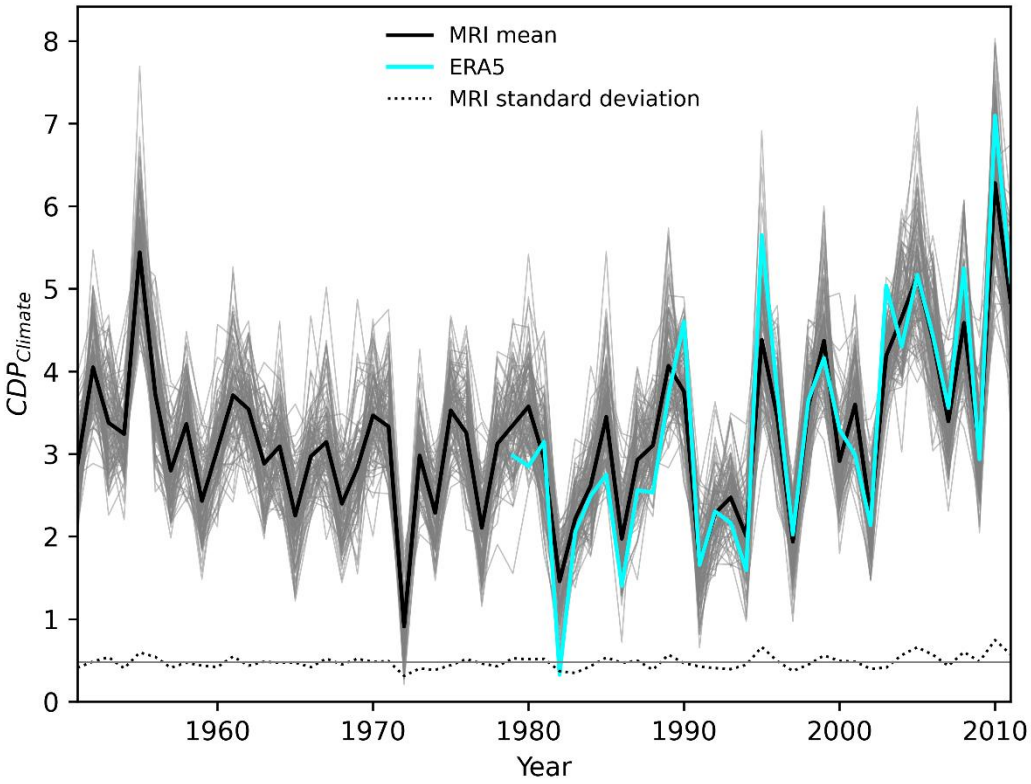

504

505 **Fig. 6** Timeseries of $CDP_{Climate}$ from ERA5 (cyan) and mean-scaled MRI (mean - black,
506 individual ensembles - grey), 1951-2011. The black dotted line is the standard deviation over
507 the 100 different ensembles for each year of the MRI data with the average value shown as a
508 grey line.

509

510

511

Figure 1

Click here to access/download;Figure;Fig1.eps

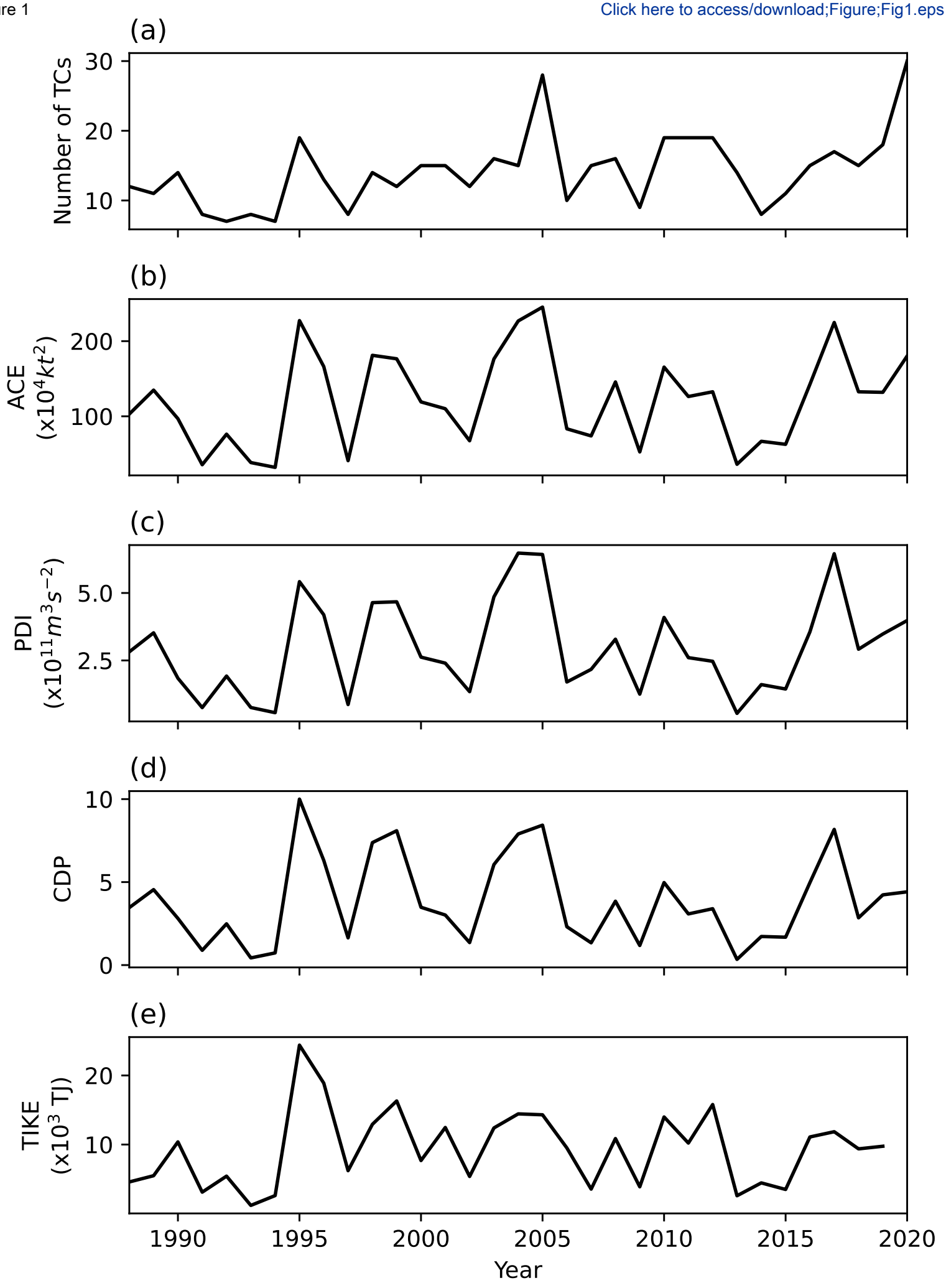

Figure 2

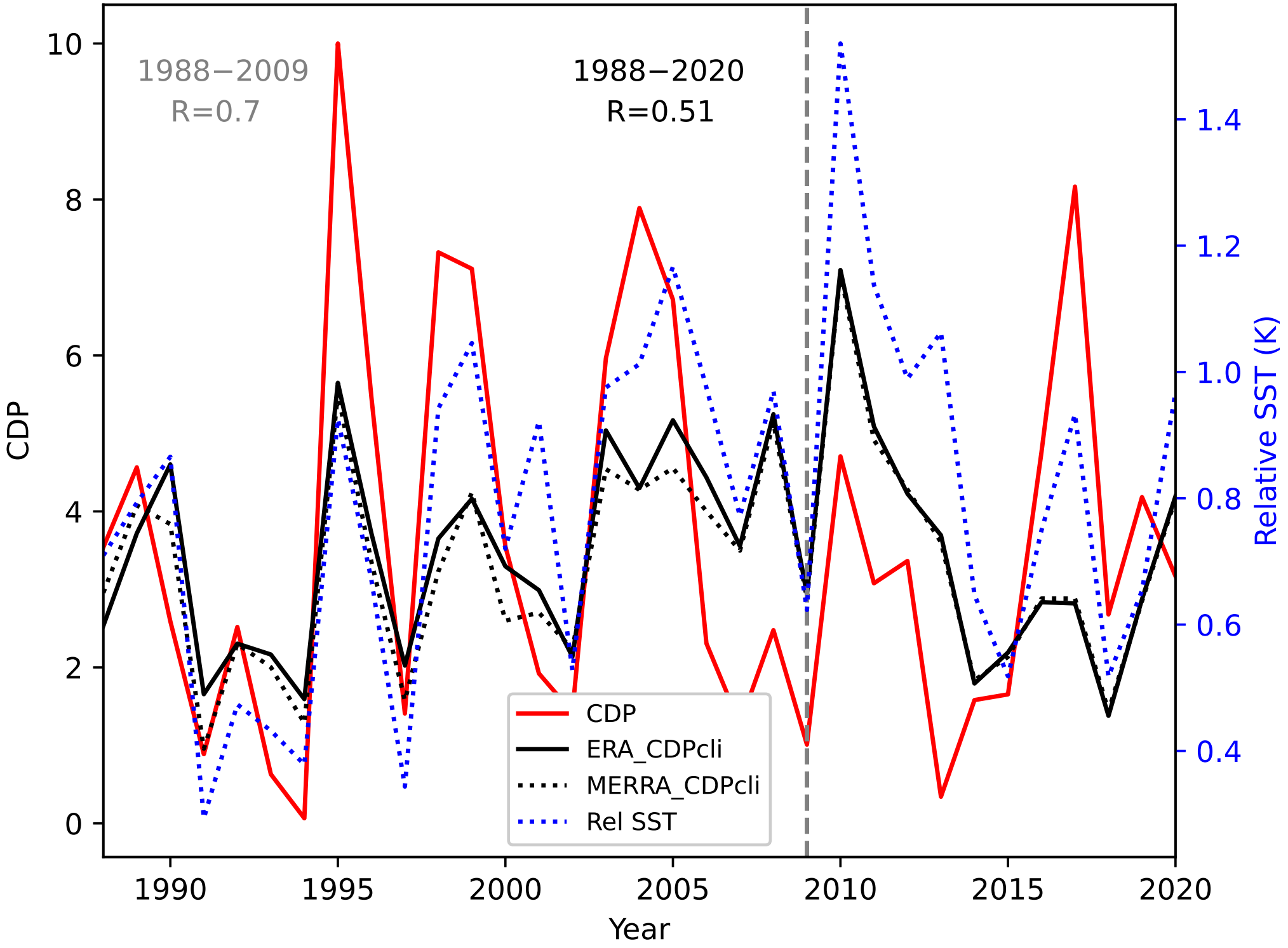

Figure 3

Click here to access/download;Figure;Fig3.eps

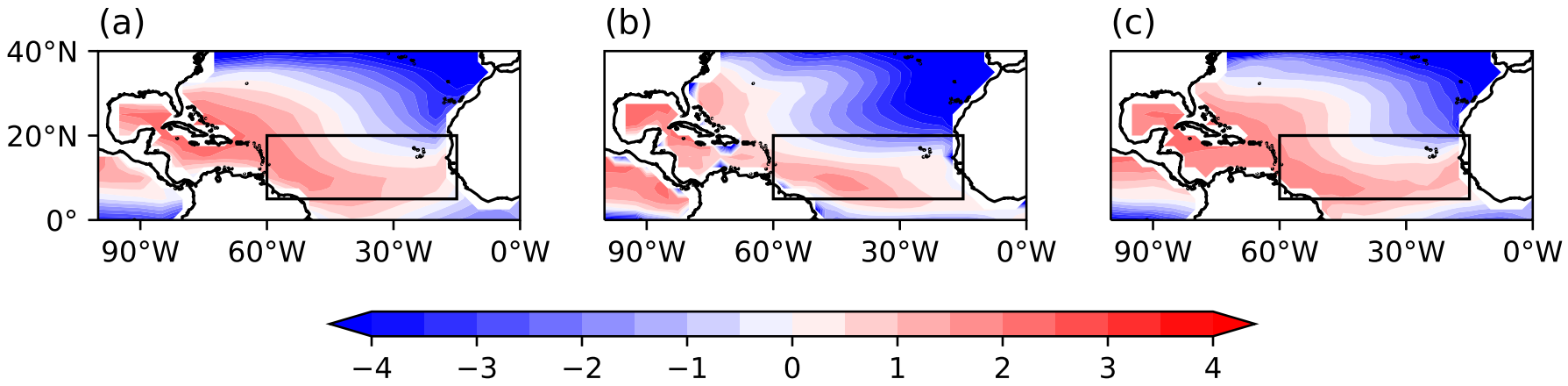

Figure 4

Click here to access/download;Figure;Fig4.eps

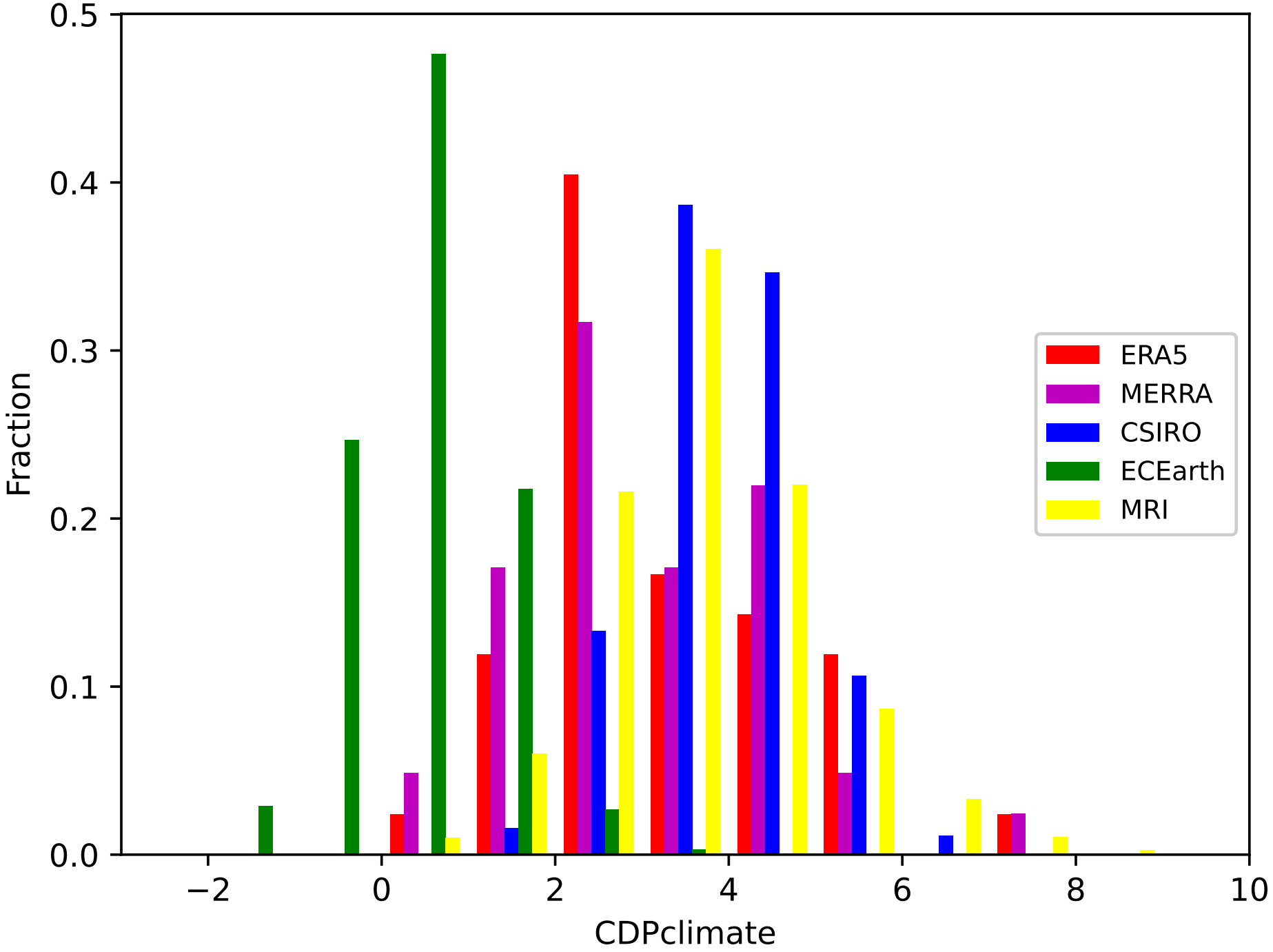

Figure 5

Click here to access/download;Figure;Fig5.eps

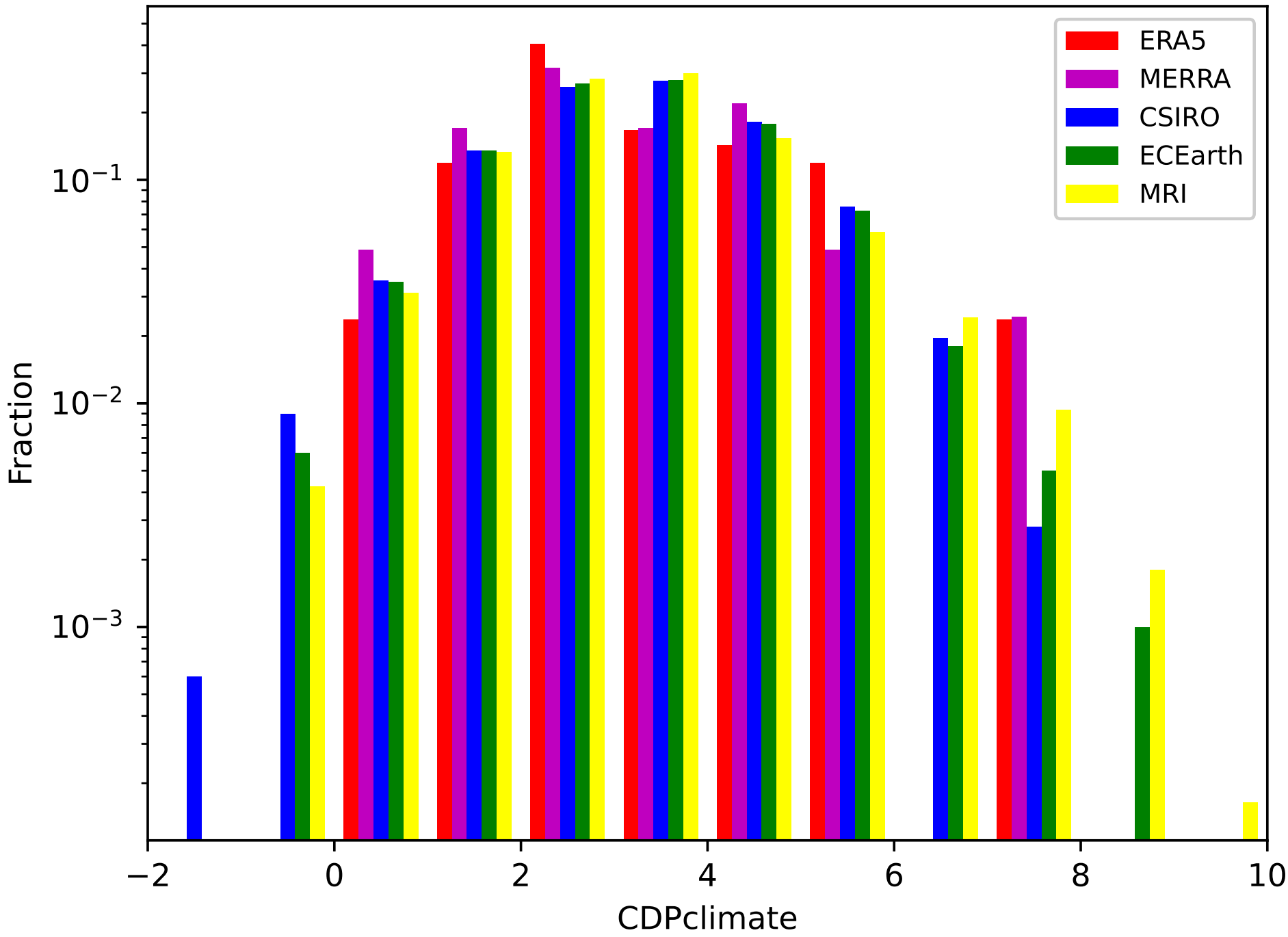

Figure 6

Click here to access/download;Figure;Fig6.eps